 doi:10.20944/preprints202204.0150.v1

Article

Genetic interaction of *Thm2* and *Thm1* Shapes Postnatal Craniofacial Bone

Erin E Bumann[1,*], Portia Hahn Leat[1], Henry H Wang[2], Brittany M Hufft-Martinez[2], Wei Wang[2] and Pamela V Tran[2,*]

[1] Department of Dental and Craniofacial Sciences, University of Missouri-Kansas City, Kansas City, MO, USA
[2] Department of Anatomy and Cell Biology, University of Kansas Medical Center, Kansas City, KS, USA
* Correspondence: bumanne@umkc.edu; Tel.: 1-816-235-6450; E.E.B.; ptran@kumc.edu; Tel.: 1-913-945-7325; P.V.T.

Abstract: Ciliopathies are genetic syndromes that link skeletal dysplasias to dysfunction of primary cilia. Primary cilia are sensory organelles synthesized by intraflagellar transport (IFT) - A and B complexes, which traffic protein cargo along a microtubular core. We have reported that deletion of IFT-A gene, *Thm2*, together with a null allele of its paralog, *Thm1*, causes a small skeleton with small mandible or micrognathia in juvenile mice. Using micro-computed tomography, here we quantify the craniofacial defects of *Thm2*$^{-/-}$;*Thm1*$^{aln/-}$ triple allele mutant mice. At postnatal day 14, triple allele mutant mice exhibit micrognathia, maxillary hypoplasia, and a decreased facial angle due to shortened maxilla, premaxilla, and nasal bones, reflecting altered development of facial anterior-posterior elements. In contrast, other ciliopathy-related craniofacial defects, such as cleft lip and/or palate, hypo-/hypertelorism, broad nasal bridge, craniosynostosis, and facial asymmetry, were not observed, suggesting development of the facial transverse dimension is intact. Calvarial-derived osteoblasts of triple allele mutant mice showed reduced bone formation *in vitro* that was ameliorated by Hedgehog agonist, SAG. Together, these data indicate that *Thm2* and *Thm1* genetically interact to regulate bone formation and sculpting of the postnatal face. The triple allele mutant mice present as a novel model to study craniofacial bone development.

Keywords: *Ttc21a*; *Ttc21b*; mouse knock-out; jaw; facial bone; viscerocranium; Hh signaling

1. Introduction

Approximately 1/5,000 births are affected by a skeletal defect. Most skeletal dysplasias are inherited, and thus, diagnosis, genetic counseling, and therapy is dependent on the underlying genetic basis[1]. For the most part, therapy is limited to surgical procedures that have unpredictable success[2].

Ciliopathies are genetic disorders of primary cilia, which are sensory organelles that are present on most mammalian cells[3, 4]. Ciliopathies cause defects in multiple organs, including the skeleton, and a subset of ciliopathies, known as the skeletal ciliopathies, cause osteochondrodysplasias [5, 6]. These include Jeune syndrome, oro-facial-digital syndromes, and Sensenbrenner syndrome, which manifest shortened long bones, narrow rib cage, polydactyly, as well as craniofacial defects. Yet craniofacial defects also occur in non-skeletal ciliopathies, such as Bardet Biedl Syndrome and Meckel Syndrome [7]. The most common ciliopathic craniofacial defects include micrognathia, cleft lip and/or palate, and variation in midfacial width including hypertelorism. Other craniofacial defects include maxillary hypoplasia, flat nasal bridge, low-set ears, prominent forehead, craniosynostosis, macrocephaly, holoprosencephaly, bifid tongue, a thin upper lip, high arched palate, epicanthal folds, and a protruding tongue. These anomalies reflect the importance of primary cilia in forming the face.

Primary cilia mediate multiple signaling pathways and thereby regulate cell behavior, tissue development and homeostasis. Primary cilia were first demonstrated to

Preprints (www.preprints.org) | NOT PEER-REVIEWED | Posted: 16 April 2022 doi:10.20944/preprints202204.0150.v1

regulate the mammalian Hedgehog (Hh) pathway[8, 9]. Subsequently, these organelles have been shown to regulate other pathways, including Wingless Integration Site (Wnt), Transforming Growth Factor Beta (TGF-β), Platelet Derived Growth Factor Receptor alpha (PDGFRα), Notch, Adenosine Monophophate-Activated Protein Kinas (AMPK), and multiple cellular processes, including proliferation, differentiation, and autophagy[10-15]. The many ciliary-mediated signaling pathways and downstream cellular processes are cell type- and developmental/age-dependent. Many of these same pathways and cellular processes are also required for bone and craniofacial development.

Primary cilia structure and function depend on intraflagellar transport (IFT), which is the bi-directional transport of structural and signaling molecules by protein complexes along a microtubular axoneme[16-18]. IFT complex B (IFT-B) proteins, powered by kinesin, transport cargo from the ciliary base to the tip in anterograde IFT, while IFT-A proteins driven by cytoplasmic dynein return proteins from the ciliary tip to the base in retrograde IFT. IFT-A proteins also mediate ciliary entry of membrane and signaling proteins. These functional differences result in contrasting phenotypes in cilia structure and often in signaling pathways in a context-dependent manner[16, 19].

Both IFT-B (*Ift80*, *Ift88*, and *Kif3a*) and IFT-A (*Thm1*, *Ift140*, *Ift144*) embryonic or juvenile mouse mutants exhibit polydactyly, shortened long bones, abnormal rib development and craniofacial defects[20-24] . Specifically, *Ift88*-null, conditional mutant, and hypomorphic mice exhibit maxillary and mandibular hypoplasia, as well as supernumerary teeth[25, 26]. Additionally, deletion of *Ift88* or *Kif3a* in neural crest cells in mice causes midfacial widening, hypertelorism, micrognathia, and cleft palate[27]. Deletion of *Thm1* in neural crest cells also causes cleft palate. These findings substantiate the importance of functional primary cilia in skeletal and craniofacial development, while underlying mechanisms and functional differences between IFT proteins continue to be challenging to elucidate.

THM1 (TPR-containing Hh modulator 1; also known as *TTC21B*) encodes an IFT-A protein and Hh modulator[28]. Mutations in *THM1* have been identified in several ciliopathies, including in Jeune syndrome, Bardet Biedl Syndrome and Meckel Syndrome, which manifest with skeletal and/or craniofacial defects [29]. *THM2* (*TTC21A*) is a paralog of *THM1* [28]. In mice, unlike loss of *Thm1*, deletion of *Thm2* alone does not cause an overt structural defect. However, deletion of *Thm2* together with a null allele of *Thm1* causes a small skeleton and micrognathia, as well as reduced *in vitro* bone formation of calvarial-derived osteoblasts [30]. To expand on the role of the *Thm2;Thm1* genetic interaction, here we characterize the craniofacial defects in greater detail and investigate the molecular pathways that underlie the osteoblast differentiation defect.

2. Materials and Methods

2.1. Mouse generation

Thm2$^{-/-}$ and *Thm2*$^{+/-}$; *Thm1*$^{aln/+}$ mice were generated and maintained on a C57BL6/J background backcrossed 5 generations as described[30]. *Thm2*$^{+/-}$;*Thm1*$^{aln/+}$ or *Thm2*$^{-/-}$; *Thm1*$^{+/+}$ females were mated to *Thm2*$^{+/-}$; *Thm1*$^{aln/+}$ males to generate *Thm2*$^{-/-}$; *Thm1*$^{aln/+}$ triple allele mutant mice. Animal procedures were conducted in accordance with KUMC-IACUC and AAALAC rules and regulations.

2.2. Scanning, Reconstruction, and Landmark Placement

Ethanol-fixed heads from postnatal day (P) 14 control and *Thm2*$^{-/-}$; *Thm1*$^{aln/+}$ mice were scanned in a Skyscan 1174 micro-computed tomography (μCT) system (Bruker, Billerica, Massachusetts, USA) at 50kVp, 800μA, with a resolution of 14μm^3. A 0.5 mm aluminum filter was used. Integration time was set to 3000ms. The scan orbit was 180°/360° with a rotation step of 0.3°.

All data were reconstructed using NRecon software version 1.7.4.2 (Bruker, Billerica, Massachusetts, USA) with Gaussian smoothing, ring-artifact reduction, and beam-hardening correction applied. Three dimensional renderings were created, and landmarks

Preprints (www.preprints.org) | NOT PEER-REVIEWED | Posted: 16 April 2022 doi:10.20944/preprints202204.0150.v1

were placed using open-source Drishti software version 2.6.5 (National Computational Infrastructure's VizLab, Canberra, Australia). Landmarks were placed on the skulls as previously published[31]. Landmarks for ear height were created and placed on the skulls since low-set ears are seen in some patients with primary ciliopathies and we wanted to determine if low-set ears were present in our *Thm2*$^{-/-}$; *Thm1*$^{aln/+}$ mice. Landmarks for ear height were placed at the superior and inferior points on the margin of the external auditory meatus. These landmarks were averaged to determine the center of the ear and then a measurement was taken from a projected plane intersecting with the top of the skull to a projected plane intersecting with the center of the ear to determine ear height as decribed[31]. All landmarks were digitized by the same researcher.

2.3. Measurements

Euclidean measurements, including angles and distances, between points were taken for all measurements. Significant measurements are listed in Supplemental Table S1 and shown in Figure 1. Projected distances between parallel planes intersecting landmarks were determined, and for all significant measurements listed in Supplemental Table S1 and shown in Figure 1. An average of the right and left measurements was used for all bilaterally paired landmarks.

Since the skulls of the *Thm2*$^{-/-}$; *Thm1*$^{aln/+}$ mice are smaller than the skulls of the control mice[30], all measurements were taken and shown as true measurements, as well as adjusted for centroid size. The centroid size of each skull and mandible was calculated using the root centroid size equation, $RCS = \sqrt{\sum_{i=1}^{n}(x_i - \bar{x})^2 + (y; -\bar{y})^2 + (z_i - \bar{z})^2}$. Then each coordinate was divided by skull centroid size before calculating distance. This makes the measurements a ratio of the entire skull size, which are then compared between groups[32].

2.4. Primary osteoblast generation and differentiation assay

Calvaria of P10 mice were used to generate primary osteoblasts[33]. Briefly, calvaria were dissected, then digested in αMEM with 2mM L-glutamine and 0.2% collagenase, Type I (Sigma, T1005)/0.05% trypsin (Sigma, C9891) for 20 minutes at 37^{0}C in a cell incubator. Media from this first digestion was discarded. An additional 4 rounds of digestion were performed. Following each of these digestions, media was collected and fetal bovine serum (FBS) was added to 10% final concentration and kept at 4^{0}C. Following the 5th digestion, all media containing digested calvaria with 10% FBS was filtered through a cell strainer with 70µm pores. The filtrate was centrifuged, pelleting the cells. Cells were resuspended in αMEM with 10% FBS, 2mM L-glutamine and penicillin/streptomycin.

Osteoblasts were plated in 24-well plates in αMEM with 10% FBS, 2mM L-glutamine and penicillin/streptomycin. Once cells reached confluency, differentiation media (αMEM, 10% FBS, 2mM L-glutamine, penicillin/streptomycin and 50µg/ml ascorbic acid and 5mM β-glycerophosphate) was applied to the cells and refreshed every 3 days over a 21-day period. To examine the effect of SAG, the differentiation media was supplemented with 0.1% DMSO or 500nM SAG throughout the 21-day period. Following the differentiation assay, cells were fixed in 10% formalin for 15 minutes, then immersed in 2% alizarin red solution for 10-15 minutes in the dark to stain bone nodules. Once the desired color intensity was obtained, cells were washed 4 times with distilled water, immersed in PBS, then fixed in 10% formalin. Wells were imaged using an EVOS® FL Auto system (ThermoFisher Scientific) attached to a CMOS color camera.

2.5. SAG treatment and qPCR

Confluent cells (differentiation day 0) or cells differentiated for 7 days were treated with 0.1% DMSO or 500nM SAG for 48 hours or throughout the 7-day differentiation period, respectively. Cells were lysed in Trizol (ThermoFisher) and stored at -80^{0}C. Once all samples were collected, RNA was extracted according to manufacturer's protocol. cDNA was made from RNA (1µg) using the Quanta Biosciences qScript cDNA mix (VWR

Preprints (www.preprints.org) | NOT PEER-REVIEWED | Posted: 16 April 2022 doi:10.20944/preprints202204.0150.v1

International). qPCR was performed in duplicate using the Quanta Biosciences Perfecta qPCR Supermix (VWR International) and a BioRad CFX Connect Real-Time PCR Detection System. Primers used were *Runx2* (Forward: 5′- CCCAGCCACCTTTACCTACA-3′; Reverse: 5′- CAGCGTCAACACCATCATTC -3′)[34]; *Col1α1* (Forward: 5′- GCATGGCCAAGAAGACATCC -3′)[35]; Reverse: 5′- CCTCGGGTTTCCACGTCTC -3′); *Tgf-β3* (Forward: 5′ GGCCAGTTCATTGTGCCCGCC 3′; Reverse: CGGTGATGACCCACGTCCCC 3′)[36]; *Smad3* (Forward: 5′ ACCAAGTGCATTACCATCC 3′; Reverse: 5′ CAGTAGATAACGTGAGGGAGCCC 3′)[35]; *Smad6* (Forward: 5′ ATTCTCGGCTGTCTCCTCCT 3′; Reverse: 5′ CCCTGAGGTAGGTCGTAGAA 3′)[37]; and housekeeping gene *Oaz1* (Forward: 5′ - GCC TGA GGG CAG TAA GGA C-3′; Reverse: 5′-GGA GTA GGG CGG CTC TGT-3′)[38].

2.6. Statistics

Unpaired, two-tailed *t* tests for comparison of two groups or Mann-Whitney tests and one-way ANOVA followed by Tukey's test for comparison of more than two groups were used to evaluate statistical significance ($p < 0.05$) using GraphPad Prism, version 9.2.0 (GraphPad, San Diego, California, USA) and reported using box-and-whisker plots, with all individual's values plotted. Effect size was calculated using Excel (Microsoft, Redmond, Washington, USA).

3. Results

3.1. Triple allele mutants have reduced skull and mandibular measurements

To determine the effect of loss of *Thm2* together with the *aln* (null) allele of *Thm1* on craniofacial development, we landmarked the μCT skull three dimensional images of P14 control and *Thm2*$^{-/-}$; *Thm1*$^{aln/+}$ littermates. When calculating for Euclidean measurements, including angular and distance measurements, multiple skull measurements were significantly decreased in the *Thm2*$^{-/-}$; *Thm1*$^{aln/+}$ mice compared to control mice (Figures 1, 2). Specifically, *Thm2*$^{-/-}$; *Thm1*$^{aln/+}$ mice showed smaller snout angle and multiple smaller distances on the skull, including anterior nasal width, inter-orbital width, inter-zygomatic arch width, intermaxillary width, inter-first molar width, nasal length, facial height, maxillary length, premaxillary length, facial region length, upper jaw length, zygomatic length, mandibular superior length, mandibular inferior length, mandibular posterior height, and ear height.

Preprints (www.preprints.org) | NOT PEER-REVIEWED | Posted: 16 April 2022 doi:10.20944/preprints202204.0150.v1

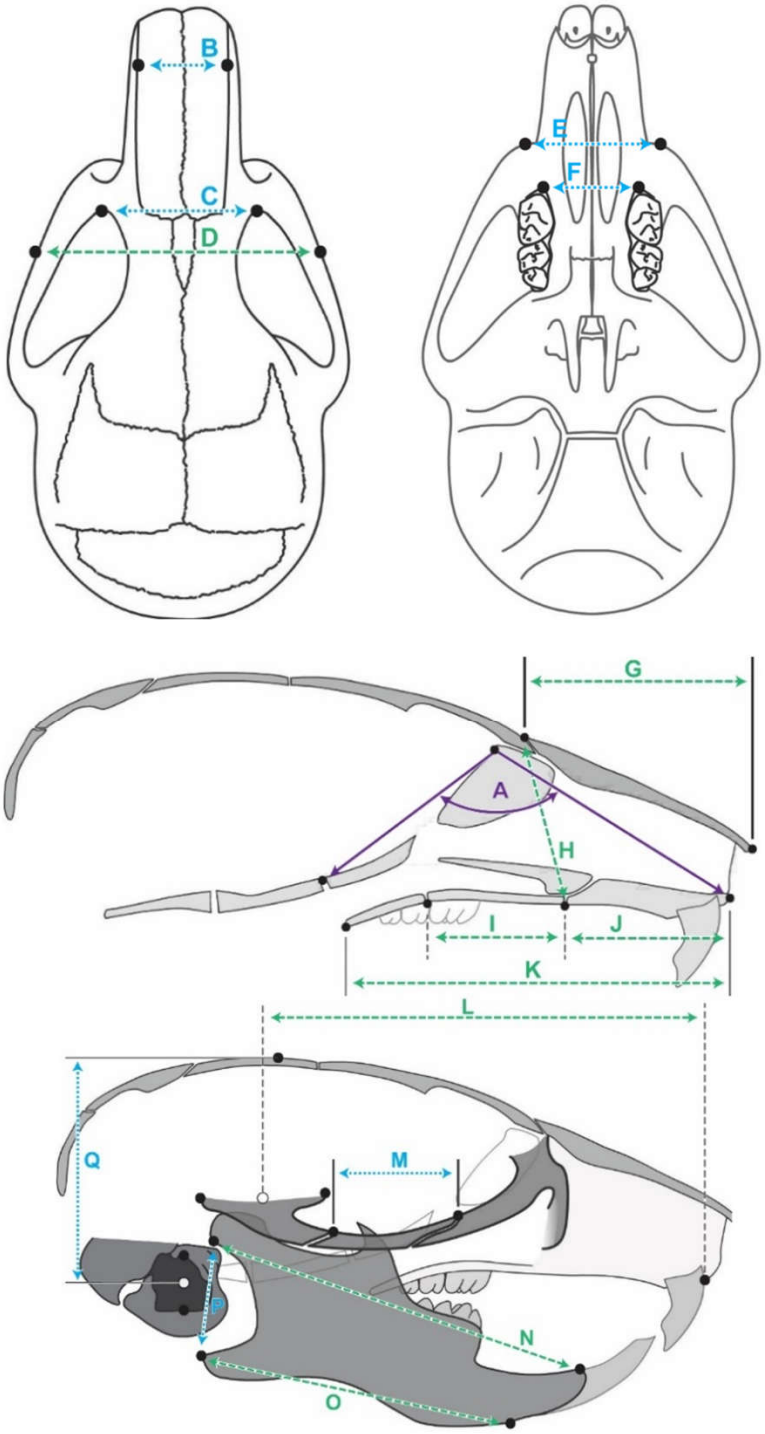

Figure 1. Schematic of craniofacial measurements and landmarks. (A) Dorsal (left) and ventral (right), as well as (B) lateral interior (top) and exterior (bottom) landmarks were placed at the points indicated by black dots. Measurements are represented by double-sided arrows. Measurements that have significant differences between control and *Thm2*$^{-/-}$; *Thm1*$^{aln/+}$ mice in true measurements are indicated by dotted blue lines. Measurements that have significant differences between control and *Thm2*$^{-/-}$; *Thm1*$^{aln/+}$ mice as both true and centroid measurements are indicated by green dashed lines. Angular measurement is indicated by solid purple lines. (A) Snout angle, (B) Anterior nasal width, (C) Inter-orbital width, (D) Inter-zygomatic arch width, (E) Inter-maxillary width, (F) Inter-(1st)molar width, (G) Nasal length, (H) Facial height, (I) Maxillary length, (J) Premaxillary length, (K) Facial region length, (L) Upper jaw length, (M) Zygomatic length, (N) Mandibular superior & (O) inferior length, (P) Mandibular posterior height and (Q) Ear height.

Preprints (www.preprints.org) | NOT PEER-REVIEWED | Posted: 16 April 2022 doi:10.20944/preprints202204.0150.v1

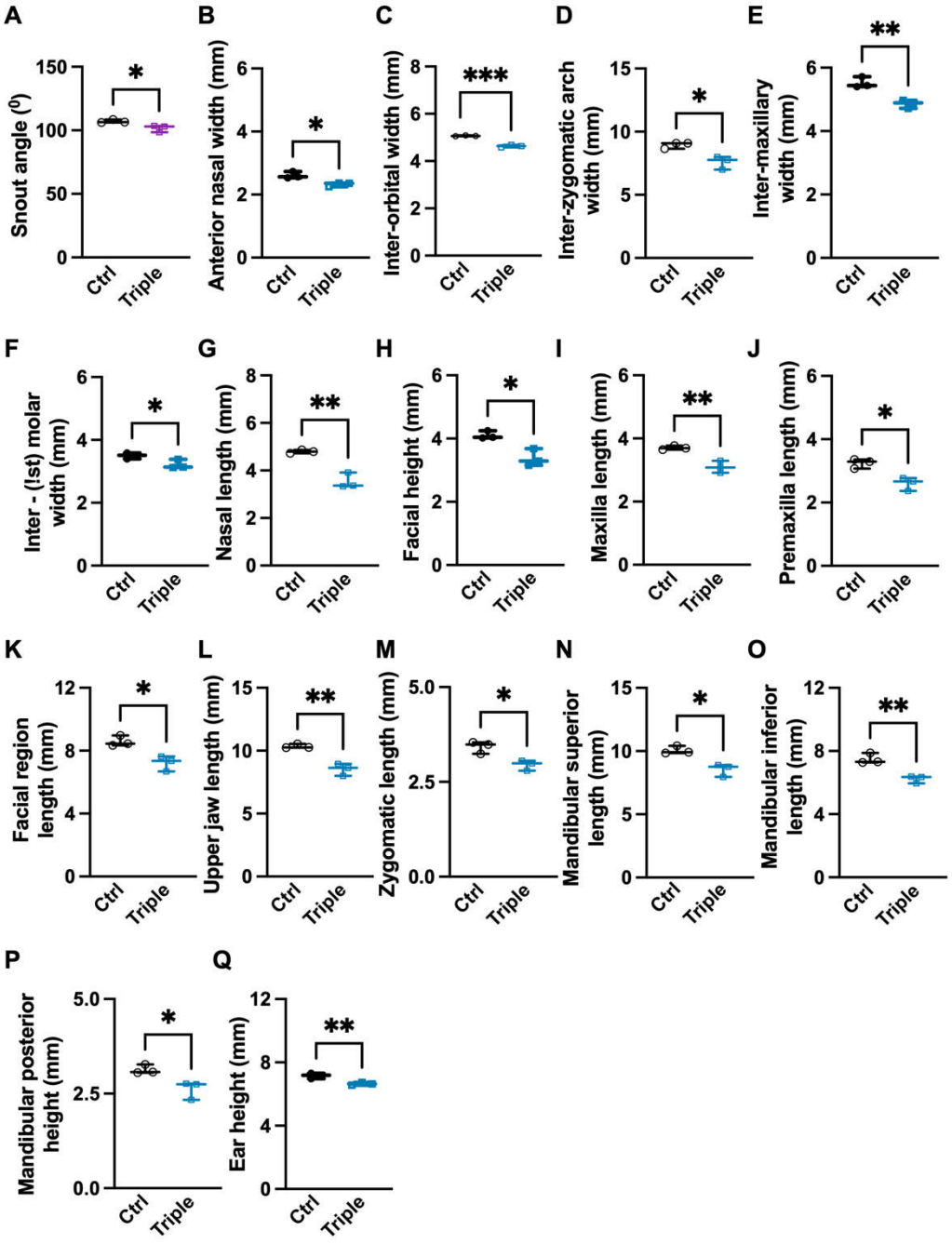

Figure 2. Significantly smaller true measurement differences in *Thm2*$^{-/-}$; *Thm1*$^{aln/+}$ mice. True measurements of control (Ctrl) and *Thm2*$^{-/-}$; *Thm1*$^{aln/+}$ (Triple) mutant (A) snout angle; (B) anterior nasal width; (C) inter-orbital width; (D) inter-zygomatic arch width; (E) inter-maxillary width; (F) inter-(1st) molar width; (G) nasal length; (H) facial height; (I) maxillary length; (J) premaxillary length; (K) facial region length; (L) upper jaw length; (M) zygomatic length; (N) mandibular superior length; (O) mandibular inferior length; (P) mandibular posterior height; (Q) ear height. n=3. Data points represent individual mice. Bars represent mean ± SEM. Statistical significance was determined using unpaired *t*-tests. *p<0.05; **p<0.01; ***p<0.001.

We next analyzed skull and mandibular centroid sizes. *Thm2*$^{-/-}$; *Thm1*$^{aln/+}$ mice did not exhibit smaller skull centroid size than control mice (Figure 3A). However, *Thm2*$^{-/-}$; *Thm1*$^{aln/+}$ mice did show smaller mandibular centroid size compared to control mice (Figure 3B), consistent with the small mandible phenotype we noted previously[28]. Moreover, when correcting for skull centroid size, *Thm2*$^{-/-}$; *Thm1*$^{aln/+}$ mice showed smaller Euclidean distance measurements compared to control mice, including inter-zygomatic arch

Preprints (www.preprints.org) | NOT PEER-REVIEWED | Posted: 16 April 2022 doi:10.20944/preprints202204.0150.v1

width, nasal length, facial height, maxillary length, premaxillary length, facial region length, upper jaw length, and mandibular superior and inferior lengths (Figures 4A-4I). Effect sizes for these measurements were negative representing the diminution in size (Figure 4J). Reduced distances in these parameters indicate maxillary hypoplasia and micrognathia in *Thm2*$^{-/-}$; *Thm1*$^{aln/+}$ mice.

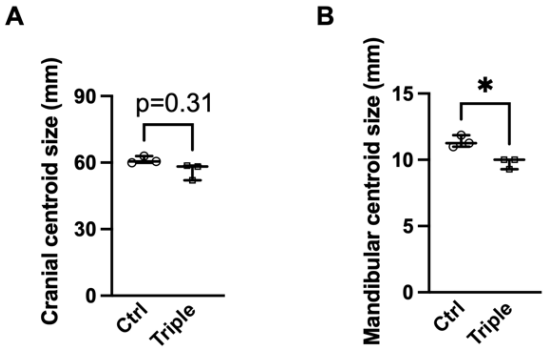

Figure 3. Centroid size differences in *Thm2*$^{-/-}$; *Thm1*$^{aln/+}$ mice. (A) Cranial centroid size and (B) Mandibular centroid size. n=3. Data points represent individual mice. Bars represent mean ± SEM. Statistical significance was determined using unpaired *t*-tests. ($p<0.05$).

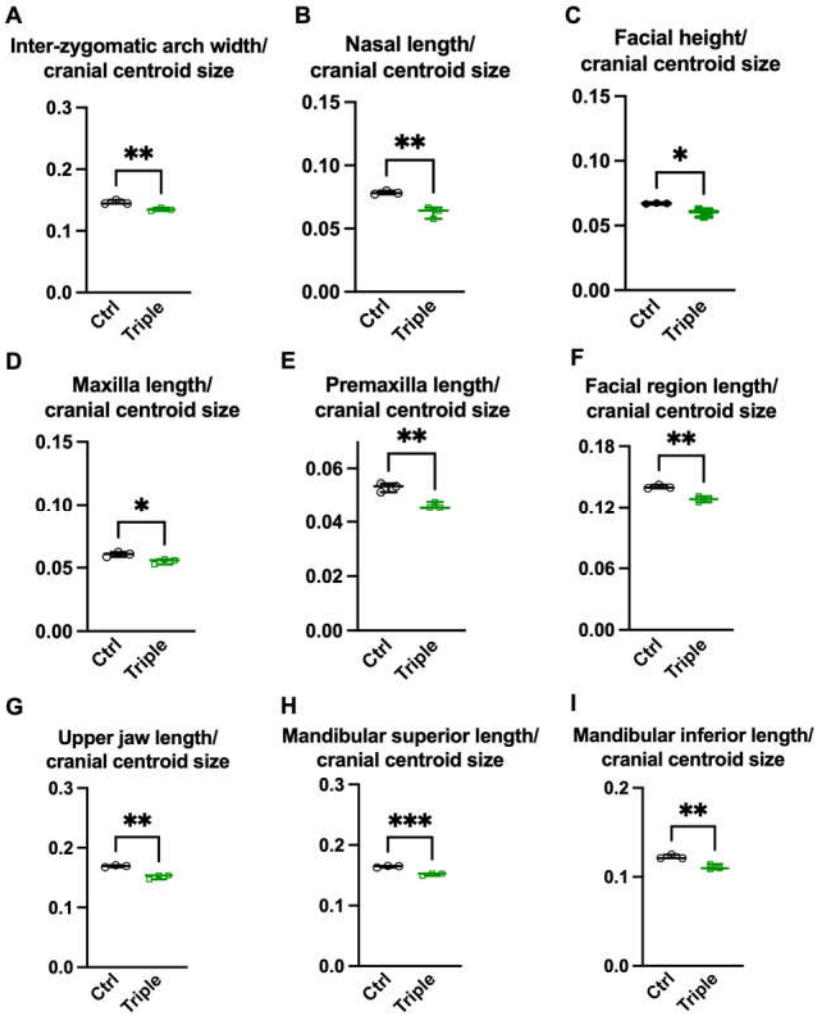

J Measurement	Effect Size
Inter-zygomatic arch width	-4.11
Nasal length	-14.12
Facial height	-24.47
Maxilla length	-3.75
Premaxilla length	-5.14
Facial region length	-8.03
Upper Jaw length	-13.91
Mandibular superior length	-11.18
Mandibular inferior length	-6.04

Figure 4. Significantly smaller measurement differences relative to centroid size in *Thm2*$^{-/-}$; *Thm1*$^{aln/+}$ mice. When correcting for centroid size, triple allele mutant mice have smaller (A) inter-zygomatic arch width; (B) nasal length; (C) facial height; (D) maxillary length; (E) premaxillary

Preprints (www.preprints.org) | NOT PEER-REVIEWED | Posted: 16 April 2022 doi:10.20944/preprints202204.0150.v1

length; (F) facial region length; (G) upper jaw length; (H) mandibular superior length; (I) mandibular inferior length. (J) Effect size of measurements in (A-I). n=3. Data points represent individual mice. Bars represent mean ± SEM. Statistical significance was determined using unpaired *t*-tests. *p<0.05; **p<0.01; ***p<0.001.

3.2. Hedgehog agonist enhances in vitro bone formation of calvarial-derived Thm2$^{-/-}$; Thm1$^{aln/+}$ osteoblasts

Using an *in vitro* osteoblast differentiation assay in which osteoblasts are differentiated to form bone nodules, we previously observed that triple allele mutant osteoblasts derived from calvaria have reduced bone formation[30]. We have also observed that deletion of one allele of *Gli2* creates and exacerbates the small skeleton phenotype in *Thm2*$^{-/-}$ and *Thm2*$^{-/-}$; *Thm1*$^{aln/+}$ juvenile mice, respectively, suggesting that loss of *Thm2* sensitizes bone development to the Hedgehog (Hh) pathway[30]. We therefore assessed the roles of *Gli2* and of Hh agonist, SAG, on *in vitro* differentiation of *Thm2*$^{-/-}$; *Thm1*$^{aln/+}$ calvarial-derived osteoblasts. As expected, formation of bone nodules by the triple allele mutant cells was reduced at differentiation day 21. However, treatment with SAG enhanced bone formation of both control and triple allele mutant cells (Figure 5A). Additionally, consistent with *Gli2* deficiency exacerbating the triple allele mutant small phenotype *in vivo*[30], loss of one allele of *Gli2* in triple allele mutant cells worsened the *in vitro* bone formation defect, which was ameliorated by SAG (Figure 5B). These data indicate that increased Hh signaling can offset the impaired bone formation of *Thm2*$^{-/-}$; *Thm1*$^{aln/+}$ cells.

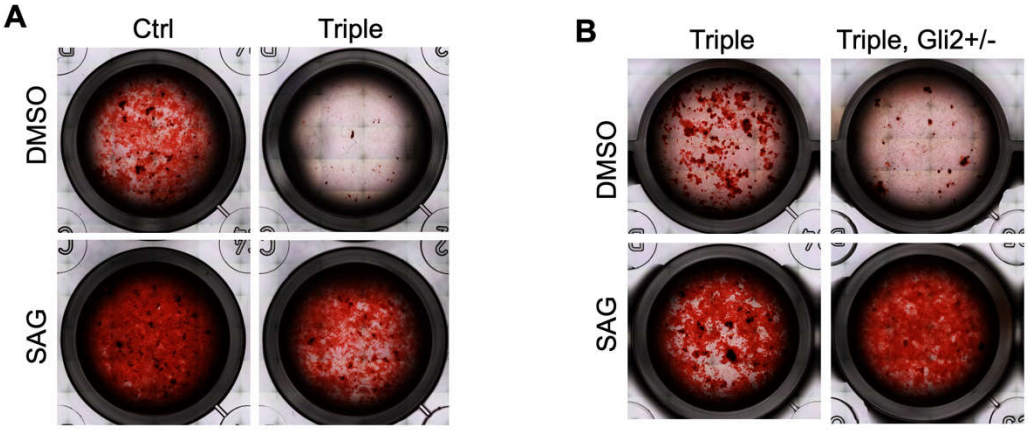

Figure 5. Amelioration of *in vitro* bone formation defect in *Thm2*$^{-/-}$; *Thm1*$^{aln/+}$ osteoblasts by Hh agonist. Images of bone nodules on day 21 of an *in vitro* differentiation assay using calvarial-derived osteoblasts of P10 (A) control and *Thm2*$^{-/-}$; *Thm1*$^{aln/+}$ littermates and (B) *Thm2*$^{-/-}$; *Thm1*$^{aln/+}$ and *Thm2*$^{-/-}$; *Thm1*$^{aln/+}$; *Gli2*$^{+/-}$ littermates. Media was supplemented with either DMSO (control) or Hh agonist (SAG) throughout the differentiation assay. n=4 control, n=4 triple, n=2 triple; *Gli2*$^{+/-}$ from 3 litters.

To determine molecular mechanisms underlying the triple allele mutant *in vitro* bone formation defect, we analyzed transcript levels of early osteoblast differentiation markers, *Runx2* and *Col1α1*, as well as components of the TGF-β signaling pathway, including *Tgf-β3*, *Smad3*, and *Smad6*, which is an inhibitory molecule of the pathway. Over 7 days of differentiation, triple allele mutant cells show a trend toward increased *Runx2* (Figure 6A). Additionally, *Col1α1* is increased in triple allele mutant cells relative to control cells at differentiation day (DD) 7 (Figure 6B). Addition of SAG to the triple allele mutant cells caused an immediate trend toward increased *Runx2* and *Col1α1* and increased *Smad3* relative to control cells (DD0), an effect which did not continue to DD7 (Figures 6A-6D). From DD0 to DD7, inhibitory *Smad6* increased and was elevated at DD7 in triple allele mutant cells relative to control cells (Figure 6E). Addition of SAG from DD0 to DD7 reduced this effect. Taken together, these data suggest that prior to differentiation, triple allele mutant osteoblasts have a heightened response to SAG. Additionally, despite some

Preprints (www.preprints.org) | NOT PEER-REVIEWED | Posted: 16 April 2022 doi:10.20944/preprints202204.0150.v1

differences in *Col1α1* and *Smad6* transcript levels, the lack of reduction in any of the transcripts examined suggests that early stages of osteoblast differentiation in triple allele mutant cells are largely intact.

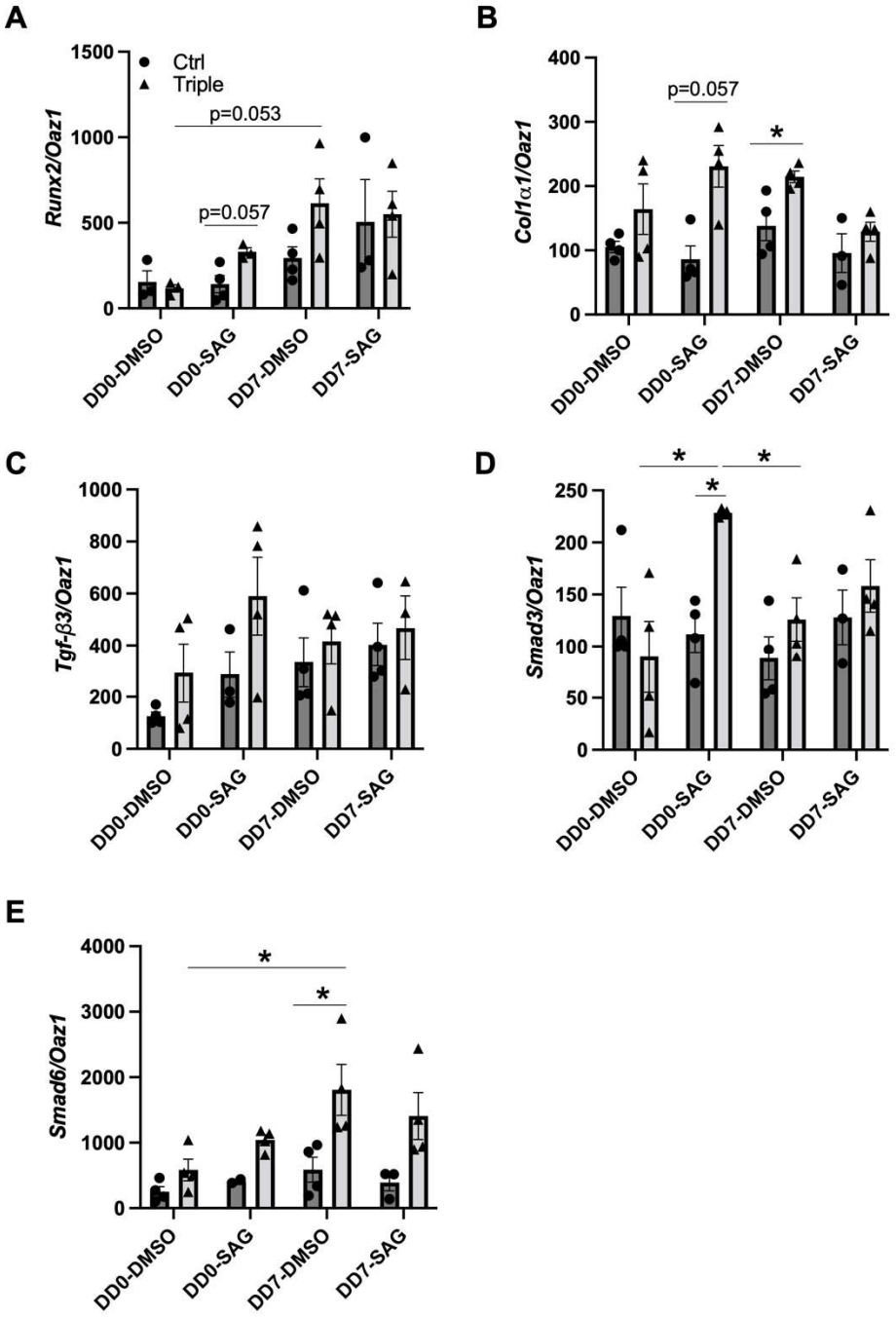

Figure 6. Transcripts of *Thm2*$^{-/-}$; *Thm1*$^{aln/+}$ calvarial-derived osteoblasts. qPCR for (A) *Runx2*; (B) *Col1α1*; (C) *Tgf-β3*; (D) *Smad3*; (E) *Smad6*, using RNA extracts of P10 control and *Thm2*$^{-/-}$; *Thm1*$^{aln/+}$ calvarial-derived osteoblasts at differentiation day 0 (DD0) or DD7 treated with either DMSO or SAG. n=4 control, n=4 triple allele mutant from 3 litters. Data points represent individual mice. Bars represent mean ± SEM. Statistical significance was determined using Mann-Whitney tests for comparison between control and triple allele mutant samples within a treatment group and using one-way ANOVA followed by Tukey's test for comparison between treatment groups for control or triple allele mutant samples, respectively . *p<0.05.

4. Discussion

 doi:10.20944/preprints202204.0150.v1

Osteogenesis is a multi-step process that involves induction, proliferation, condensation, differentiation, matrix (osteoid) deposition, vascularization, mineralization, and remodeling. Two types of ossification - intramembranous and endochondral - develop the skeleton. During intramembranous ossification, mesenchymal progenitor cells differentiate directly into osteoblasts, which then mature into osteocytes. In contrast, during endochondral ossification, mesenchymal progenitor cells differentiate into chondrocytes, which undergo maturation, before being replaced by invading osteoblasts. While intramembranous ossification develops most bones of the cranial vault and facial skeleton, including the maxilla and distal mandible, endochondral ossification develops most of the remaining skeleton, including long bones, the cranial base and proximal mandible[39]. Micrognathia in triple allele mutant mice may reflect that both intramembranous and endochondral ossification are disrupted in facial development[40]. In support of an endochondral ossification defect, we have previously found that the *Thm2*$^{-/-}$;*Thm1*$^{aln/+}$ mice show a chondrocyte differentiation defect in the tibia[30]. However, since intramembranous and endochondral ossification converge on osteoblasts, it is also possible that the micrognathia in *Thm2*$^{-/-}$;*Thm1*$^{aln/+}$ mice is due to an osteoblast differentiation defect.

Once mesenchymal cells in intramembranous ossification and osteo-chondro progenitor cells in endochondral ossification commit to the osteoblast lineage, osteoblast differentiation can be described in three stages based on cell cycle stage and gene expression[40]. *Runx2* expression is required for progenitors to commit to the osteoblast lineage. Subsequently, in the first stage of differentiation, osteoblasts proliferate and express collagen type I, TGF-β receptors and osteopontin. In the second stage of differentiation, osteoblasts exit the cell cycle and express alkaline phosphatase and collagen type I for maturation of the extracellular matrix. In the third stage of differentiation, mature osteoblasts secrete osteocalcin and mineralize the extracellular matrix. Although some variations in transcript levels of early osteoblast markers were observed in triple allele mutant cells relative to control cells, lack of deficiency in *Runx2*, *Col1α1* and *Tgf-β3* transcripts in triple allele mutant osteoblasts suggests the *in vitro* bone differentiation defect likely occurs at later stages of differentiation.

Additionally, osteoblast differentiation is modulated by multiple signaling pathways, including the Hh pathway. Mice null for Indian Hedgehog (*Ihh*), a ligand of the pathway, show an absence of osteoblast differentiation[41]. Similarly, *Ift80* conditional knock-out mice show loss of Hh signaling and impaired osteoblast differentiation[42]. While Hh signaling has been shown to be important in early stages of osteoblast differentiation by inducing *Runx2* expression[43], the addition of SAG throughout the 21 days of *in vitro* differentiation enhanced bone nodule formation not only in control cells, but also in triple allele mutant cells. This suggests that SAG also enhances later stages of differentiation, countering the triple allele mutant bone formation defect.

Recently, micrognathia in the *ta*^{2} chick mutant was shown to result from incomplete osteoblast differentiation as well as increased bone resorption [44]. An earlier than normal commitment of progenitors to the osteoblast lineage reflected by increased *Runx2* and *Col1α1* in the mandibular prominence of the *ta*^{2} chick mutant, similar to what we observed in triple allele mutant osteoblasts *in vitro*, resulted in incomplete differentiation of osteoblasts, indicated by decreased levels of alkaline phosphatase in the *ta*^{2} mandibles of older embryos. Additionally, in *ta*^{2} mandibles, expression of bone remodeling markers was increased, indicating increased bone resorption. This substantiates that bone resorption levels are inversely proportional to jaw size in avian embryos [45].

Another potential mechanism that may contribute to maxillary and mandibular hypoplasia are defects in development of the cranial base. In a comparative study of normal and anencephalic human fetuses, cranial base lengths were reduced in anencephalic fetuses and correlated with maxillary protrusion[46]. Additionally, the cranial base angle negatively correlated with mandibular protrusion. Thus, future analyses of the triple allele mutant cranial base sutures, which form from endochondral ossificiation, would be informative.

While the triple allele mutant craniofacial defects - shortened nasal, mandibular and maxillary lengths - appeared specific to anterior-posterior measurements, other ciliopathy-related craniofacial defects, such as cleft lip and/or palate, hypo-/hypertelorism, broad nasal bridge, craniosynostosis, and facial asymmetry, were not observed. This suggests development of the facial transverse dimension is not disrupted. This may be explained if the facial anterior-posterior defects do arise from defects of the cranial base. Another possibility could be that the precise temporal and spatial regulation of signaling pathways by individual ciliary proteins and their interactions regulate development of specific facial elements[27]. While the interactive THM2 and THM1 function appears to regulate facial anterior-posterior elements primarily, IFT88 and KIF3A regulate both facial anterior-posterior and transverse dimensions[27].

In summary, this study demonstrates that genetic interaction between *Thm2* and *Thm1* in mice shapes the postnatal face and presents a novel model to study the etiology of craniofacial ciliopathies.

Supplementary Materials: Table S1: Euclidean and Projected Measurements

Author Contributions: Conceptualization, E.E.B. and P.V.T.; methodology, E.E.B., P.H.L., and P.V.T.; investigation, E.E.B., P.H.L., H.H.W., B.M.H-M, W.W., P.V.T; writing—original draft preparation, E.E.B., P.H.L., and P.V.T.; writing—review and editing, E.E.B. and P.V.T; supervision, E.E.B. and P.V.T.; funding acquisition, E.E.B. and P.V.T. All authors have read and agreed to the published version of the manuscript.

Funding: This research was funded by a pilot grant from the Kansas City Consortium on Musculoskeletal Diseases.

Data Availability Statement: Not applicable.

Conflicts of Interest: The authors declare no conflict of interest.

References

1. Krakow, D. and D.L. Rimoin, *The skeletal dysplasias.* Genet Med, 2010. **12**(6): p. 327-41.
2. Poyner, S.E. and W.T. Bradshaw, *Jeune syndrome: considerations for management of asphyxiating thoracic dystrophy.* Neonatal Netw, 2013. **32**(5): p. 342-52.
3. Xiao, Z., et al., *Cilia-like structures and polycystin-1 in osteoblasts/osteocytes and associated abnormalities in skeletogenesis and Runx2 expression.* J Biol Chem, 2006. **281**(41): p. 30884-95.
4. Song, B., et al., *Development of the post-natal growth plate requires intraflagellar transport proteins.* Dev Biol, 2007. **305**(1): p. 202-16.
5. Tobin, J.L. and P.L. Beales, *The nonmotile ciliopathies.* Genet Med, 2009. **11**(6): p. 386-402.
6. McInerney-Leo, A.M., et al., *Short-rib polydactyly and Jeune syndromes are caused by mutations in WDR60.* Am J Hum Genet, 2013. **93**(3): p. 515-23.
7. Cortes, C.R., V. Metzis, and C. Wicking, *Unmasking the ciliopathies: craniofacial defects and the primary cilium.* Wiley Interdiscip Rev Dev Biol, 2015. **4**(6): p. 637-53.
8. Huangfu, D., et al., *Hedgehog signalling in the mouse requires intraflagellar transport proteins.* Nature, 2003. **426**(6962): p. 83-7.
9. Eggenschwiler, J.T. and K.V. Anderson, *Cilia and developmental signaling.* Annu Rev Cell Dev Biol, 2007. **23**: p. 345-73.
10. Corbit, K.C., et al., *Kif3a constrains beta-catenin-dependent Wnt signalling through dual ciliary and non-ciliary mechanisms.* Nat Cell Biol, 2008. **10**(1): p. 70-6.
11. Schneider, L., et al., *PDGFRalphaalpha signaling is regulated through the primary cilium in fibroblasts.* Curr Biol, 2005. **15**(20): p. 1861-6.
12. Clement, C.A., et al., *TGF-beta signaling is associated with endocytosis at the pocket region of the primary cilium.* Cell Rep, 2013. **3**(6): p. 1806-14.
13. Ezratty, E.J., et al., *A role for the primary cilium in Notch signaling and epidermal differentiation during skin development.* Cell, 2011. **145**(7): p. 1129-41.
14. Miceli, C., et al., *The primary cilium and lipophagy translate mechanical forces to direct metabolic adaptation of kidney epithelial cells.* Nat Cell Biol, 2020. **22**(9): p. 1091-1102.
15. Wheway, G., L. Nazlamova, and J.T. Hancock, *Signaling through the Primary Cilium.* Front Cell Dev Biol, 2018. **6**: p. 8.
16. Goetz, S.C., P.J. Ocbina, and K.V. Anderson, *The primary cilium as a Hedgehog signal transduction machine.* Methods Cell Biol, 2009. **94**: p. 199-222.
17. Veland, I.R., et al., *Primary cilia and signaling pathways in mammalian development, health and disease.* Nephron Physiol, 2009. **111**(3): p. p39-53.
18. Valente, E.M., et al., *Primary cilia in neurodevelopmental disorders.* Nat Rev Neurol, 2014. **10**(1): p. 27-36.
19. Christensen, S.T. and C.M. Ott, *Cell signaling. A ciliary signaling switch.* Science, 2007. **317**(5836): p. 330-1.

20. Herron, B.J., et al., *Efficient generation and mapping of recessive developmental mutations using ENU mutagenesis.* Nat Genet, 2002. **30**(2): p. 185-9.
21. Miller, K.A., et al., *Cauli: a mouse strain with an Ift140 mutation that results in a skeletal ciliopathy modelling Jeune syndrome.* PLoS Genet, 2013. **9**(8): p. e1003746.
22. Ashe, A., et al., *Mutations in mouse Ift144 model the craniofacial, limb and rib defects in skeletal ciliopathies.* Hum Mol Genet, 2012. **21**(8): p. 1808-23.
23. Rix, S., et al., *An Ift80 mouse model of short rib polydactyly syndromes shows defects in hedgehog signalling without loss or malformation of cilia.* Hum Mol Genet, 2011. **20**(7): p. 1306-14.
24. Haycraft, C.J., et al., *Intraflagellar transport is essential for endochondral bone formation.* Development, 2007. **134**(2): p. 307-16.
25. Murcia, N.S., et al., *The Oak Ridge Polycystic Kidney (orpk) disease gene is required for left-right axis determination.* Development, 2000. **127**(11): p. 2347-55.
26. Zhang, Q., et al., *Loss of the Tg737 protein results in skeletal patterning defects.* Dev Dyn, 2003. **227**(1): p. 78-90.
27. Schock, E.N., et al., *A tissue-specific role for intraflagellar transport genes during craniofacial development.* PLoS One, 2017. **12**(3): p. e0174206.
28. Tran, P.V., et al., *THM1 negatively modulates mouse sonic hedgehog signal transduction and affects retrograde intraflagellar transport in cilia.* Nat Genet, 2008. **40**(4): p. 403-10.
29. Davis, E.E., et al., *TTC21B contributes both causal and modifying alleles across the ciliopathy spectrum.* Nat Genet, 2011. **43**(3): p. 189-96.
30. Allard, B.A., et al., *Thm2 interacts with paralog, Thm1, and sensitizes to Hedgehog signaling in postnatal skeletogenesis.* Cell Mol Life Sci, 2021. **78**(7): p. 3743-3762.
31. Vora, S.R., E.D. Camci, and T.C. Cox, *Postnatal Ontogeny of the Cranial Base and Craniofacial Skeleton in Male C57BL/6J Mice: A Reference Standard for Quantitative Analysis.* Front Physiol, 2015. **6**: p. 417.
32. Klingenberg, C.P., *Size, shape, and form: concepts of allometry in geometric morphometrics.* Dev Genes Evol, 2016. **226**(3): p. 113-37.
33. Dallas, S.L., et al., *Dual role for the latent transforming growth factor-beta binding protein in storage of latent TGF-beta in the extracellular matrix and as a structural matrix protein.* J Cell Biol, 1995. **131**(2): p. 539-49.
34. Kim, J.H., et al., *Downregulation of Runx2 by 1,25-Dihydroxyvitamin D(3) Induces the Transdifferentiation of Osteoblasts to Adipocytes.* Int J Mol Sci, 2016. **17**(5).
35. Berthet, E., et al., *Smad3 binds Scleraxis and Mohawk and regulates tendon matrix organization.* J Orthop Res, 2013. **31**(9): p. 1475-83.
36. Palazuelos, J., M. Klingener, and A. Aguirre, *TGFbeta signaling regulates the timing of CNS myelination by modulating oligodendrocyte progenitor cell cycle exit through SMAD3/4/FoxO1/Sp1.* J Neurosci, 2014. **34**(23): p. 7917-30.
37. Estrada, K.D., et al., *Smad6 is essential to limit BMP signaling during cartilage development.* J Bone Miner Res, 2011. **26**(10): p. 2498-510.
38. de Jonge, H.J., et al., *Evidence based selection of housekeeping genes.* PLoS One, 2007. **2**(9): p. e898.
39. Yang, J., et al., *The Hedgehog signalling pathway in bone formation.* Int J Oral Sci, 2015. **7**(2): p. 73-9.
40. Biosse Duplan, M., et al., *Meckel's and condylar cartilages anomalies in achondroplasia result in defective development and growth of the mandible.* Hum Mol Genet, 2016. **25**(14): p. 2997-3010.
41. Long, F., et al., *Ihh signaling is directly required for the osteoblast lineage in the endochondral skeleton.* Development, 2004. **131**(6): p. 1309-18.
42. Yuan, X., et al., *Ciliary IFT80 balances canonical versus non-canonical hedgehog signalling for osteoblast differentiation.* Nat Commun, 2016. **7**: p. 11024.
43. Shimoyama, A., et al., *Ihh/Gli2 signaling promotes osteoblast differentiation by regulating Runx2 expression and function.* Mol Biol Cell, 2007. **18**(7): p. 2411-8.
44. Bonatto Paese, C.L., et al., *Ciliopathic micrognathia is caused by aberrant skeletal differentiation and remodeling.* Development, 2021. **148**(4).
45. Ealba, E.L., et al., *Neural crest-mediated bone resorption is a determinant of species-specific jaw length.* Dev Biol, 2015. **408**(1): p. 151-63.
46. Esenlik, E., et al., *Cephalometric investigation of craniomaxillofacial structures during the prenatal period: a cadaver study.* Am J Orthod Dentofacial Orthop, 2014. **145**(2): p. 217-27.